Three-dimensional diamagnetic particle deflection in ferrofluid microchannel flows

Litao Liang, Junjie Zhu, and Xiangchun Xuan[a)]
Department of Mechanical Engineering, Clemson University, Clemson, South Carolina 29634-0921, USA

(Received 19 May 2011; accepted 7 July 2011; published online 4 August 2011)

Magnetic field-induced particle manipulation is a promising technique for biomicrofluidics applications. It is simple, cheap, and also free of fluid heating issues that accompany other common electric, acoustic, and optical methods. This work presents a fundamental study of diamagnetic particle motion in ferrofluid flows through a rectangular microchannel with a nearby permanent magnet. Due to their negligible magnetization relative to the ferrofluid, diamagnetic particles experience negative magnetophoresis and are repelled away from the magnet. The result is a three-dimensionally focused particle stream flowing near the bottom outer corner of the microchannel that is the farthest to the center of the magnet and hence has the smallest magnetic field. The effects of the particle's relative position to the magnet, particle size, ferrofluid flow rate, and concentration on this three-dimensional diamagnetic particle deflection are systematically studied. The obtained experimental results agree quantitatively with the predictions of a three-dimensional analytical model. © *2011 American Institute of Physics*.
[doi:10.1063/1.3618737]

I. INTRODUCTION

A variety of force fields have been demonstrated to implement particle manipulations (e.g., focusing,[1] trapping, concentration,[2] separation, and sorting[3,4]) in microfluidic devices, among which electric,[5–7] acoustic,[8–10] magnetic,[11–13] and optical[14–16] forces are the most often used ones. While each of these methods has advantages and disadvantages, magnetic field-induced particle control via permanent magnets is potentially the simplest and cheapest one. Moreover, this method is free of fluid heating issues that accompany electric, acoustic, and optical techniques. It is based on magnetophoresis which directs particles either along or against the magnetic field gradient. In the former, magnetic particles suspended in nonmagnetic solutions experience *positive* magnetophoresis and are attracted towards a magnet where the magnetic field is the highest.[17] This phenomenon has been exploited to selectively trap and continuously sort cells or biomolecules out of a heterogeneous mixture by labeling the target bioparticles with functionalized magnetic beads.[18–21] It has also been demonstrated to separate paramagnetic red blood cells from blood without magnetic labeling.[22,23] This direction has been and is still the main focus of current research activities on magnetic microfluidics. Readers interested in this research area are referred to recent review articles from Pamme,[11] Liu *et al.*,[24] and Gijs *et al.*[25]

In contrast, much less work has been reported on *negative* magnetophoresis, where diamagnetic particles, which cover the majority of synthetic and biological particles, suspended in magnetic solutions are repelled away from the magnet due to the magnetic buoyancy force.[26] So far, two types of magnetic solutions have been used for this purpose, i.e., paramagnetic salts and ferrofluids. Common paramagnetic solutions such as $MnCl_2$ and $GdCl_3$ have a weak

[a)]Author to whom correspondence should be addressed. Electronic mail: xcxuan@clemson.edu. Tel.: 864-656-5630. Fax: 864-656-7299.

magnetic susceptibility.[27] Therefore, the salt concentration must be high in order to induce sufficient magnetophoretic particle motion, which, however, renders the paramagnetic solution non-biocompatible.[28] Alternatively, strong magnet(s) (e.g., a superconducting magnet[29]) must be used to provide large magnetic fields or the magnet(s) must be brought very close to the suspended diamagnetic particles[30] in order to generate large magnetic field gradients. Either of these requirements greatly increases the difficulty for magnetic particle manipulation within on-chip planar microchannels. Significant contributions to this area have been made by research groups around the world such as Pamme in UK,[28,29,31] Park in South Korea,[32,33] Suwa and Watarai in Japan,[34–36] and Whitesides in USA.[27,30,37–39] Their works are reviewed in a recent article from Suwa and Watarai.[40]

Ferrofluids are opaque colloidal suspensions of magnetic nanoparticles (made of magnetite, Fe_3O_4, and usually of 10 nm in diameter) in pure water or organic oil with surfactants coated to prevent agglomerations.[41] The synthesis of biocompatible ferrofluids has been recently demonstrated feasible by Yellen's[42] and Koser's[43] groups through the use of appropriate stabilizing surfactants. Ferrofluids usually have a magnetic susceptibility that is several orders of magnitude larger than paramagnetic solutions. Therefore, regular permanent and electric magnets normally suffice to induce *negative* magnetophoresis for manipulating diamagnetic particles with varying sizes.[44,45] Current research activities in this area can be divided into two directions, according to the feature of the external magnetic field. In the first direction, a uniform magnetic field is imposed (e.g., via a permanent magnet that is much larger in size than the microfluidic chip) to magnetize surface-patterned micromagnets, around which strong magnetic field gradients can then be generated. This method has been used to pattern, concentrate, and sort submicron and even nanometer diamagnetic particles in ferrofluids.[46–54] The second direction in ferrofluids-based particle manipulation research is to utilize the inherent non-uniformity in the magnetic field around a magnet to induce magnetophoresis. This approach has been mainly applied to manipulate diamagnetic microparticles including the self-assembly[42,55] and continuous-flow separation of particles and cells.[43,56]

In this work, we perform a comprehensive study of diamagnetic particle motion in ferrofluid microchannel flows using a combined experimental and theoretical method. The particle transport is investigated in both the horizontal and the vertical planes of a rectangular microchannel, which demonstrates a three-dimensional particle deflection due to the induced negative magnetophoresis. We also develop a three-dimensional analytical model to understand the observed particle behavior in ferrofluid flows, which is validated by the acquired experimental results. This work is based on a recent paper from Zhu *et al.*[57] who studied the widthwise deflection of hydrodynamically focused diamagnetic particles in a rectangular microchannel. Their experimental results agree closely with the predictions of a two-dimensional analytical model where particles are assumed to be in touch with the bottom channel wall.

II. EXPERIMENT

A. Device fabrication

Fig. 1(a) shows a picture of the microfluidic device used in our experiment. The straight microchannel (filled with the black-brown ferrofluid) is 2 cm long, 200 μm wide, and 70 μm deep. It was fabricated with PDMS using the standard soft lithography method, and the detail is given elsewhere.[58] Prior to the dispense of liquid PDMS over the channel master, a prism was positioned 500 μm away from the edge of the microchannel in order for the side-view imaging and was fixed to the substrate using a sticky tape. The cured PDMS along with the embedded prism was then carved out and bonded to a glass slide forming the microfluidic chip. In the half of the chip without the prism, part of the PDMS was cut out wherein a neodymium (NdFeB) permanent magnet (B221, K&J Magnetics, Inc.) was placed with its bottom surface in contact with the glass slide. The distance between the magnet and the microchannel can be varied during the experiment. The magnet has a dimension of $3.176 \times 3.176 \times 1.588$ (mm) thick, and is magnetized through thickness which is perpendicular to the microchannel or the flow direction in our experiment.

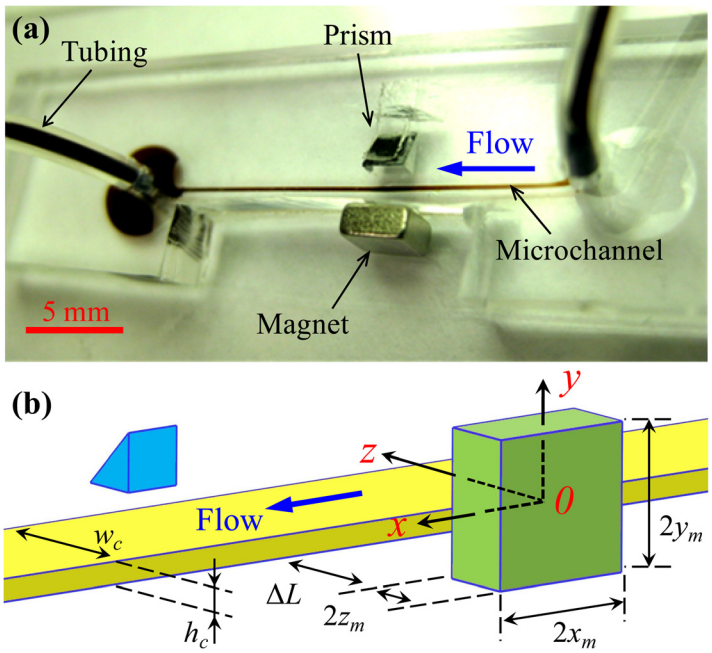

FIG. 1. Picture of the microfluidic device used in the experiment (a) and schematic of the magnet-microchannel system with coordinates and dimensions indicated (b). The coordinate system originates from the center of the permanent magnet whose magnetization direction is in line with coordinate z. Note that the magnet and the microchannel are both in direct contract with the substrate, so that the center of the magnet is not aligned with the central height of the microchannel.

B. Preparation of particle suspensions

EMG 408 ferrofluid was purchased from Ferrotec (USA) Corp. It contains 1.2% magnetic nanoparticles in volume with a reported viscosity of 1.2×10^{-3} kg/m/s,[57] and has a saturation magnetization of 5252 A/m (corresponding to 6.6 mT as per the manufacturer). Green fluorescent polystyrene particles of 2.2 μm, 5 μm, and 10 μm in diameters were obtained from Duke Scientific Corp. They are all packaged as 1% solids in water with size non-uniformity being less than 5%. Each type of these diamagnetic microparticles was re-suspended in either the original or a diluted ferrofluid to a final concentration of about 1×10^6 particles/ml. The $0.5\times$ (i.e., 0.6% magnetic nanoparticles in volume) and $0.25\times$ (i.e., 0.3% vol.) dilutions were made by mixing the original ferrofluid with the same and the triple volume of de-ionized water, respectively. The suspension of 5 μm particles in $0.5\times$ ferrofluid was used as a solution of reference in our experiment.

C. Particle manipulation and visualization

The particle suspensions in ferrofluids were driven through the microchannel by an infusion syringe pump (NE-300, New Era Pump Systems, Inc., NY). Teflon tubing (1622L, Upchurch Scientific) was used to connect the pump to the channel and to transfer the solution out of the channel. Particle motion was visualized and recorded using an inverted microscope (Nikon Eclipse TE2000U, Nikon Instruments, Lewisville, TX) equipped with a CCD camera (Nikon DS-Qi1Mc). The obtained images were then processed using the Nikon imaging software (NIS-Elements AR 2.30).

III. THEORY

A. Magnetic force

The magnetic "buoyancy" force, $\mathbf{F}_m$, on a diamagnetic particle suspended in a magnetic fluid is given by[12,13]

$$\mathbf{F}_m = -V_p \mu_0 (\mathbf{M}_f \bullet \nabla)\mathbf{H} \tag{1}$$

where V_p is the volume of the particle, $\mu_0 = 4\pi \times 10^{-7}$ H/m is the permeability of free space, $\mathbf{M}_f$ is the effective magnetization of the ferrofluid, and $\mathbf{H}$ is the magnetic field at the particle center. Note that Eq. (1) is valid only when the variation of the applied magnetic field over the particle volume can be neglected. This assumption is fulfilled in the current work as the permanent magnet is distant from the microchannel and the particles are small in size. The former fact also enables us to neglect the influence of the magnetic field on the concentration of magnetic nanoparticles in the ferrofluid, i.e., the volume fraction of nanoparticles, ϕ, is assumed homogeneous in the following analysis.

The magnetization of ferrofluids, $\mathbf{M}_f$, is collinear with the static magnetic field, $\mathbf{H}$, produced by a permanent magnet, and its magnitude, M_f, can be determined using the Langevin function, $L(\alpha)$, if the volume fraction of magnetic nanoparticles, ϕ, is low,[59]

$$\frac{M_f}{\phi M_d} = L(\alpha) = \coth(\alpha) - \frac{1}{\alpha}, \tag{2}$$

$$\alpha = \frac{\pi d^3 \mu_0 M_d H}{6 k_B T}, \tag{3}$$

where $M_d = 4.379 \times 10^5$ A/m is the saturation moment of the magnetic nanoparticles as calculated from the manufacturer-provided saturation magnetization of the ferrofluid, M_{sat} (= 5252 A/m for EMG 408 with $\phi = 1.2\%$), through $M_d = M_{sat}/\phi$. Other symbols in Eq. (3) include H, the magnetic field magnitude, d, the average diameter of the magnetic nanoparticles, k_B, the Boltzmann constant, and T, the ferrofluid or particle temperature. The components of $\mathbf{M}_f$ along the three directions, M_i ($i = x, y, z$) can be related to those of $\mathbf{H}$, i.e., H_i ($i = x, y, z$), through Eq. (4),

$$M_i = M_f \frac{H_i}{H}. \tag{4}$$

Theoretically, the ferrofluid (and the diamagnetic microparticles as well) should disturb the external magnetic field due to its dissimilar permeability from free space. However, this perturbation is essentially small for dilute ferrofluids. Therefore, we can employ Furlani's analytical model[60] to determine the three-dimensional magnetic field, $\mathbf{H} = (H_x, H_y, H_z)$, of a rectangular magnet whose magnetization direction is in line with z coordinate,

$$H_x(x,y,z) = \frac{M_s}{4\pi} \sum_{i=1}^{2} \sum_{j=1}^{2} (-1)^{i+j} \ln \left\{ \frac{(y-y_1) + \left[(x-x_i)^2 + (y-y_1)^2 + (z-z_j)^2\right]^{1/2}}{(y-y_2) + \left[(x-x_i)^2 + (y-y_2)^2 + (z-z_j)^2\right]^{1/2}} \right\}, \tag{5}$$

$$H_y(x,y,z) = \frac{M_s}{4\pi} \sum_{i=1}^{2} \sum_{j=1}^{2} (-1)^{i+j} \ln \left\{ \frac{(x-x_1) + \left[(x-x_1)^2 + (y-y_i)^2 + (z-z_j)^2\right]^{1/2}}{(x-x_2) + \left[(x-x_2)^2 + (y-y_i)^2 + (z-z_j)^2\right]^{1/2}} \right\}, \tag{6}$$

$$H_z(x,y,z) = \frac{M_s}{4\pi} \sum_{i=1}^{2} \sum_{j=1}^{2} \sum_{k=1}^{2} (-1)^{i+j+k} \tan^{-1} \left\{ \frac{(x-x_i)(y-y_j)}{(z-z_k)\left[(x-x_i)^2 + (y-y_j)^2 + (z-z_k)^2\right]^{1/2}} \right\}, \tag{7}$$

where $M_s = 1.05 \times 10^6$ A/m is the residual magnetization of the permanent magnet as calculated from the residual magnetic flux density, B_s (= 1.32 T as per the manufacturer) through $M_s = B_s/\mu_0$. Other symbols involved in the magnetic field equations are $x_1 = x_m$, $x_2 = -x_m$, $y_1 = y_m$, $y_2 = -y_m$, $z_1 = z_m$, and $z_2 = -z_m$ where x_m, y_m, and z_m represent one half of the dimensions of

TABLE I. List of the parameters used in the analytical model. Some of the parameters are varied in the experiment, and their specific values are referred to the text.

Parameter		Description	Value	Unit
Magnet	M_s	Residual magnetization	1.05×10^6	A/m
	$2x_m$	Length	3.176	mm
	$2y_m$	Height	3.176	mm
	$2z_m$	Thickness (polar direction)	1.588	mm
	ΔL	Distance between the magnet and the channel edge	1.33	mm
Ferrofluid	ϕ	Volume fraction of magnetic nanoparticles	1.20% for original	
	M_d	Saturation moment of magnetic nanoparticles	4.379×10^5	A/m
	D	Mean diameter of magnetic nanoparticles	10	Nm
	η	Dynamic viscosity	1.2×10^{-3} for original	kg/m/s
Diamagnetic particles	$2a$	Particle diameter	Three sizes used: 2.2, 5, and 10	μm
Microchannel	w_c	Channel width	200	μm
	h_c	Channel height	70	μm
	Q	Volume flow rate	480	µl/h

the magnet in the x, y, and z directions, respectively. The coordinates and dimensions for the magnet-microchannel system are illustrated in Fig. 1(b). Note that the coordinate system originates from the center of the magnet.

B. Magnetic deflection

The presence of the negative sign in Eq. (1) indicates that the magnetic force, $\mathbf{F}_m$, directs diamagnetic particles in ferrofluids along the direction of decreasing magnetic field. Using Eqs. (5)–(7), we obtained the magnetic field distribution with the channel for the current magnet-microchannel system (see Fig. 1). Table I summarizes the parameters used in the calculation. Fig. 2 shows the magnetic field contours in the horizontal plane at $y = -y_m + h_c/2$ with h_c the microchannel height (left plot) and the vertical plane at $x = 0$ (right plot) of the microchannel (see Fig. 1(b) for the coordinates). It is evident that the permanent magnet generates magnetic field gradients in all three directions. Specifically in the horizontal plane (i.e., x-z plane, left),

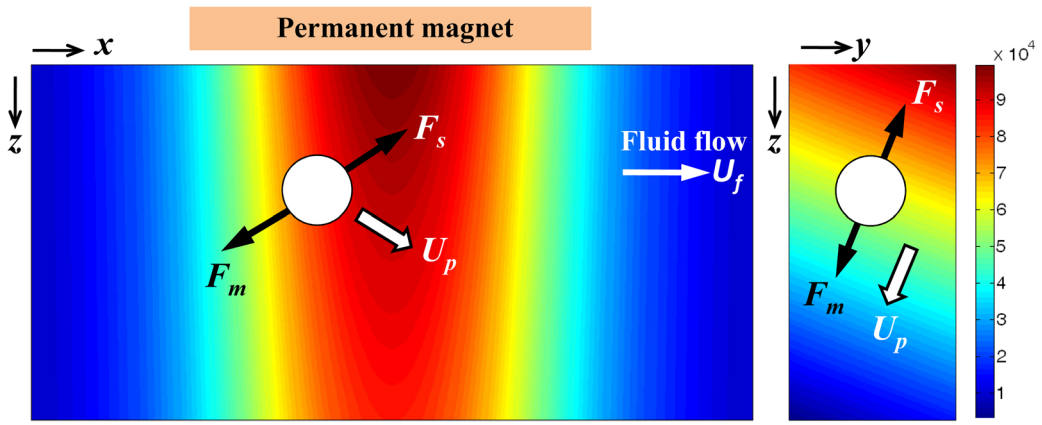

FIG. 2. Force analyses on a diamagnetic particle in ferrofluid field flow in the horizontal (left, partial view) and vertical (right, i.e., the channel cross-sectional view) planes of the microchannel. The background colors show the contours of the magnetic field magnitude (in the unit of H/m) in the absence of the diamagnetic particle. The magnet-microchannel configuration is referred to Fig. 1. The microchannel and magnet are not drawn to scale.

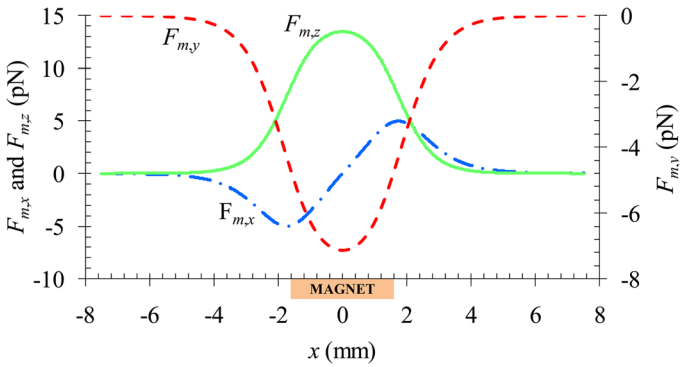

FIG. 3. Axial variations of the three components of the magnetic force, $\mathbf{F}_m$, along the centerline of the microchannel. The location of the permanent magnet is highlighted in the plot.

diamagnetic particles should be deviated from the x-direction ferrofluid flow and deflected along the positive z direction toward the channel's sidewall that is farther from the magnet. Meanwhile in the vertical plane (i.e., y-z plane, right), the particles should also be deflected along the negative y direction toward the bottom channel wall, i.e., downwards from the magnet center. These two phenomena are schematically illustrated in Fig. 2 via the force analysis on a single particle, where $\mathbf{F}_s$ denotes the Stokes drag force.

The above analysis is also supported by the axial distribution of the magnetic force, $\mathbf{F}_m$, on a 5 μm diamagnetic particle along the channel centerline as demonstrated in Fig. 3. Other parameters involved in the calculation are summarized in Table. I. The z-component force, $F_{m,z}$, and the y-component force, $F_{m,y}$, acquire a positive and a negative value, respectively, within about 3 mm distance before and after the magnet (i.e., -5 mm $< x <$ $+5$ mm). They both reach the extreme when the particle is on the center-plane of the magnet, i.e., $x = 0$. Similarly, the x-component magnetic force, $F_{m,x}$, also obtains a non-zero value in the same range of x. It, however, varies from negative (which hinders the particle motion) in the upstream half of the magnet to positive (which propels the particle) in the downstream half. The ultimate consequence of these negative magnetophoretic motions is a three-dimensionally focused particle stream flowing near the outer bottom corner of the microchannel, the farthest place from the center of the magnet.

The magnetic *deflection* of diamagnetic particles in ferrofluid flows is determined by the ratio of the particle velocities, $\mathbf{U}_p$, perpendicular and parallel to the flow,

$$deflection_i = \frac{U_{p,i}}{U_{p,x}} = \frac{U_{m,i}}{U_f + U_{m,x}} \quad (i = y, z), \tag{8}$$

where U_f is the axial flow velocity given by[61]

$$U_f = \frac{Q\pi}{2w_c h_c}\left\{\left[1 - \frac{\cosh\left(\frac{\pi z'}{h_c}\right)}{\cosh\left(\frac{\pi w_c}{2h_c}\right)}\right]\cos\left(\frac{\pi y'}{h_c}\right) - \frac{1}{27}\left[1 - \frac{\cosh\left(\frac{3\pi z'}{h_c}\right)}{\cosh\left(\frac{3\pi w_c}{2h_c}\right)}\right]\cos\left(\frac{3\pi y'}{h_c}\right)\right\}$$
$$\times\left\{\left[1 - \frac{2h_c}{\pi w_c}\tanh\left(\frac{\pi w_c}{2h_c}\right)\right] + \frac{1}{81}\left[1 - \frac{2h_c}{3\pi w_c}\tanh\left(\frac{3\pi w_c}{2h_c}\right)\right]\right\}^{-1}, \tag{9}$$

where Q is the volume flow rate of the particle suspension through the microchannel of width w_c and height h_c. The auxiliary coordinates y' and z' originate from the center of channel cross-section and are parallel to the y and z coordinates for the magnet (see Fig. 1(b)), respectively. Note that Eq. (9) contains only the first two terms in the general formula for simplicity, which is found to cause less than 1% error.[57] Additionally, we have neglected the influence of the magnetic force on ferrofluid velocity in order to use the analytical formula in Eq. (9).

The magnetophoretic particle velocity, $\mathbf{U}_m$, in Eq. (8) can be obtained by balancing the magnetic force, $\mathbf{F}_m$, in Eq. (1) with the Stokes drag force (i.e., $\mathbf{F}_s$ in Fig. 2), yielding

$$\mathbf{U}_m = \frac{\mathbf{F}_m}{6\pi\eta a f_D} = \frac{-\mu_0 \phi a^2}{9\eta f_D} \frac{M_d L(\alpha) \nabla H^2}{H} \tag{10}$$

where η is the dynamic viscosity of the ferrofluid, a is the radius of the spherical diamagnetic particle, and f_D is the drag coefficient accounting for the particle-wall interactions.[63] Equations (1) and (2) have been used to obtain the term after the second equal sign in Eq. (10). The fraction involving magnetic field is derived based on the fact that the ferrofluid magnetization, $\mathbf{M}_f$, is collinear with the static magnetic field, $\mathbf{H}$. Therefore, the diamagnetic particle deflection should increase with increasing ferrofluid concentration, ϕ, and particle size, a. In addition, lowering the ferrofluid flow velocity (or flow rate) should also enhance the particle deflection according to Eq. (8). As the width of the microchannel is nearly three times the depth, we consider only the retardation effects from the top or the bottom wall whichever is closer to the particle. Moreover, for particle motions parallel (i.e., along the x- and z-directions, see Fig. 1(b)) and normal (i.e., along the y-direction) to the top/bottom wall, we use different formulae for f_D,[62]

$$f_{D,||} = \left[1 - \frac{9}{16}\left(\frac{a}{\delta}\right) + \frac{1}{8}\left(\frac{a}{\delta}\right)^3 - \frac{45}{256}\left(\frac{a}{\delta}\right)^4 - \frac{1}{16}\left(\frac{a}{\delta}\right)^5\right]^{-1}, \tag{11}$$

$$f_{D,\perp} = \left[1 - \frac{9}{8}\left(\frac{a}{\delta}\right) + \frac{1}{2}\left(\frac{a}{\delta}\right)^3\right]^{-1}, \tag{12}$$

where δ is the smaller value of the separation distances from the particle center to the top and the bottom channel walls, respectively.

C. Simulation of particle trajectory

Based on the above analysis, we developed a 3D analytical model to simulate the trajectory of diamagnetic particles in ferrofluid flows in response to magnetic field gradients. The instantaneous position of a particle, $\mathbf{r}_p$, was obtained by integrating the particle velocity over time, which is written as

$$\mathbf{r}_p = \mathbf{r}_0 + \int_0^t \left[\mathbf{U}_f(t') + \mathbf{U}_m(t')\right] dt', \tag{13}$$

where $\mathbf{r}_0$ is the initial location of the particle and t is the time coordinate. Note that both the fluid velocity, $\mathbf{U}_f$, and the magnetophoretic particle velocity, $\mathbf{U}_m$ are dependent on position, and so vary with time during the particle migration. We have excluded the contributions of gravity and inertia in the particle velocity in Eq. (13). As per the manufacturers, the mass densities of the original EMG 408 ferrofluid and the diamagnetic particles are 1.07×10^3 kg/m^3 and 1.05×10^3 kg/m^3, respectively, which yields a net gravity-buoyancy force of 1.28×10^{-2} pN for 5-μm diameter particles. This force is two orders of magnitude smaller than the magnetic force illustrated in Fig. 3, and can cause particle sedimentation at a speed of 0.27 μm/s at most. Hence, the gravity effects are not considered. In addition, the largest flow rate in our experiment is 960 μL/hr, equivalent to an average flow speed of 19.2 mm/s. Hence, the calculated particle Reynolds number is only 0.024 even for the biggest 10-μm diameter particles we have used. This value is at least 20 times smaller than the reported at which the cross-stream inertial particle motion is observed.[63] Therefore, particle inertia is also neglected in our analytical model.

A custom-written MATLAB® program was used to determine the particle position, $\mathbf{r}_p$, with respect to time and to plot the particle trajectory. Totally 20×10 (in the form of width $\times$ depth) evenly distributed points were picked at the entrance of the microchannel as the initial particle

positions. The integral of particle velocity over time in Eq. (13) was implemented by summing the products of the particle velocity and the time step length at each time step. A sufficiently small time step (0.1 ms) was chosen to ensure the accuracy of the computation. All parameters involved in the 3D model are listed in Table I unless otherwise stated in Sec. IV.

IV. RESULTS AND DISCUSSION

A. Confirmation of three-dimensional magnetic deflection

To confirm the three-dimensional deflection of diamagnetic particles in ferrofluid flows, we examined the particle motions with and without a permanent magnet on-chip in both the horizontal (i.e., top view, more accurately, bottom view through an inverted microscope) and vertical (i.e., side view) planes of the microchannel. In the experiment 5 μm particles were re-suspended in $0.5\times$EMG 408 ferrofluid (i.e., the original ferrofluid was diluted to its half concentration with pure water). A permanent magnet was either placed 2.2 mm away from the microchannel (i.e., $\Delta L = 2.2$ mm in Fig. 1(b)) at 2 mm upstream of the prism or simply taken away from the microfluidic chip.

Fig. 4 compares the experimentally obtained snapshot (top row) and superimposed (middle row) images with the theoretically predicted particle trajectories (bottom row) for both the top ((a1)–(a3)) and side ((b1)–(b3)) views. In the absence of the magnet, particles simply follow the x-direction ferrofluid flow and cover the channel cross-section uniformly for the tested flow rates. This is evidenced by the experimental images in Figs. 4(a1) and 4(b1), which are also indicated by the predicted particle trajectories in both view planes. However, when the magnet is on-chip, particles can only partially cover the width and depth of the channel due to magnetic deflection. Moreover, as expected, this deflection decreases with increasing flow rate in both directions as demonstrated in Figs. 4(a2), 4(a3), 4(b2), and 4(b3). We find that at a flow rate of 180 μL/hr (equivalent to an average flow speed of 3.6 mm/s), particles are depleted in the half of the channel width [Fig. 4(a2)] and depth [Fig. 4(b2)] closer to the magnet center. In contrast, particles are fully deflected in both the width and depth directions at a reduced flow rate of 45 μl/h, and focused to a single file in the outer bottom corner of the microchannel (see Figs. 4(a3) and

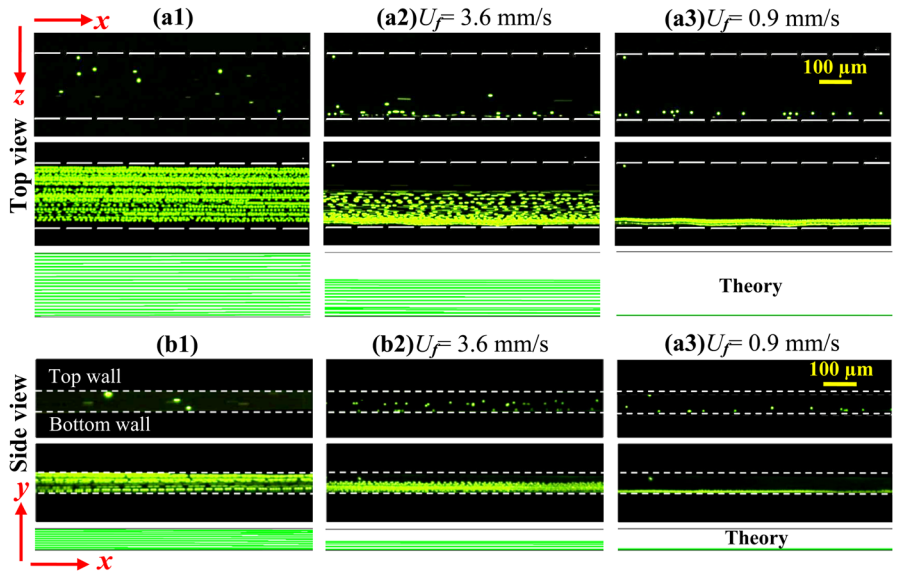

FIG. 4. Demonstration of the three-dimensional deflection of 5 μm diamagnetic particles in $0.5\times$EMG 408 ferrofluid for the cases of without magnet ((a1), (b1)) and with magnet at the flow rate of 180 μL/hr ((a2), (b2), equivalent to an average flow speed of 3.6 mm/s) and 45 μL/hr (a3, b3, 0.9 mm/s). The top, middle, and bottom rows in each panel demonstrate the snapshot image, superimposed image, and theoretically predicted trajectories of 5 μm particles, respectively. Note that the few particles in (b3) that appear to be out of the downward deflected particle stream were immobilized on the channel sidewall.

4(b3)), the farthest from the center of the magnet. These experimental observations match the theoretical predictions qualitatively. A quantitative study of the factors that affect the diamagnetic particle deflection in ferrofluid microchannel flows is presented in the following section.

B. Systematic study of horizontal magnetic deflection

1. Evolution of particle deflection

To understand how the magnetic deflection evolves when particles approach and move by the permanent magnet, we studied 5 μm particle motions in 0.5 × EMG 408 ferrofluid in a row of five observation windows along the channel length with reference to the position of the magnet: 2.5 mm upstream (Window 1), 0 mm before (Window 2), center (Window 3), 0 mm after (Window 4), and 2 mm downstream (Window 5). The relative positions of these observation windows to the magnet can also be read from the x-coordinate values in Fig. 5(b). The magnet was placed 1.33 mm away from the microchannel, and this distance was fixed in the rest of the experiments presented below. Note that the larger magnet-channel distance (2.2 mm) in Fig. 4 is used for the purpose of lowering the ferrofluid flow speed at the full-width particle deflection, which was found to facilitate side-viewing the particle motion in the channel depth direction. Top-view images were taken for investigating the diamagnetic particle deflection in the horizontal direction of the microchannel only.

Fig. 5(a) shows the top-view images in the five observation windows at a flow rate of 480 μL/hr. One can see that particles follow the fluid flow in Window 1 without noticeable deviations, but acquire an apparent deflection in Window 2 when they approach the magnet. This magnetic deflection grows continuously to about one half of the channel width as particles move through the magnet region, which is clearly demonstrated by the images from Windows 3 and 4. It vanishes when particles move into Window 5. This trend can be explained by the axial variations of the magnetic force, $F_{m,z}$, in Fig. 3. We also note that the acquired diamagnetic particle deflection in Fig. 5(a) (Window 5) is comparable to that in Fig. 4(a2) while at a much larger flow rate. This is attributed to the stronger magnetic field and field gradients within the channel in the former situation as a result of the smaller magnet-channel distance. A quantitative comparison between the experimentally measured (symbols) and theoretically predicted (curve) widths of the focused particle stream is shown in Fig. 5(b). The experimental error in

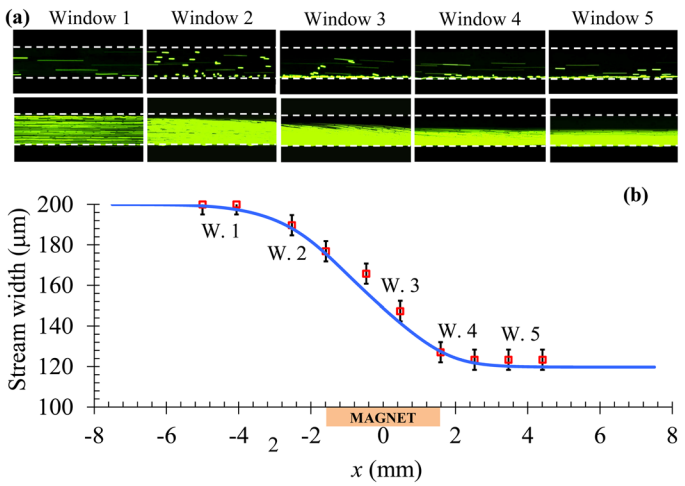

FIG. 5. Lengthwise evolution of the diamagnetic deflection of 5 μm particles in 0.5 × EMG 408 ferrofluid at a flow rate of 480 μL/hr (equivalent to an average flow speed of 9.6 mm/s): top-view snapshot (top row) and superimposed (bottom row) images in five consecutive observation windows along the channel length (a); comparison of the experimentally measured (symbols) and theoretically predicted (curve) widths of the particle stream along the floe direction (b). The relative positions of the five observation windows (labeled as W.1-W.5) to the permanent magnet can be read from their x-coordinate values in (b).

measuring the stream width is estimated to be about 10 μm. A good agreement is obtained for the results in all five observation windows.

2. Effect of flow rate

As demonstrated in Figs. 4(a2), 4(a3), 4(b2), and (b3), the diamagnetic particle deflection diminishes with increasing flow rate. A more detailed study of this flow effect is given in Fig. 6. Three flow rates ($Q = 240$, 480, and 960 μL/hr, symbols, see also the insets for superimposed top-view images) were tested for 5 μm particle suspension in 0.5 × EMG 408 ferrofluid, and the obtained widths of the particle streams in Window 5 (i.e., 2 mm after the magnet, see Fig. 5) are compared to the theoretically predicted curve. We find that particles can be fully deflected when the flow rate is 240 μL/hr or less, and the eventual width of the particle stream can be down to the particle diameter in principle. This and as well the particle stream widths at 480 and 960 μL/hr are predicted with good agreement by the analytical model. As indicated in Eq. (8), the particle *deflection* (i.e., channel width minus the particle stream width) should be inversely proportional to the flow rate if the fluid velocity is much greater than the axial magnetophoretic particle velocity. This condition is fulfilled as the induced magnetic velocity is on the order of 100 μm/s while the lowest flow velocity we used in this experiment is 4.8 mm/s (for 240 μL/hr). The relationship between the particle stream width and the inverse of the flow rate is shown in the inset graph of Fig. 6, which is indeed approximately linear as expected. The deviation is likely associated with the three-dimensional magnetic deflection and the non-uniform fluid velocity over the channel cross-section.

3. Effect of particle size

Equation (10) indicates that the induced magnetophoretic velocity is proportional to particle diameter squared. As a result, the magnetic deflection should be a quadratic function of particle diameter if the fluid velocity is much greater than the axial magnetophoretic particle velocity. In order to verify this size effect, we tested the magnetic deflection of diamagnetic particles of three different diameters, 2.2, 5, and 10 μm, in 0.5 × EMG 408 ferrofluid at a flow rate of 480 μL/hr. Fig. 7 compares the experimental data (symbols and top-view snapshot images) with the theoretical curve for the stream width of particles of different diameters 2 mm after the magnet. Note that the horizontal axis is the particle diameter squared. For 2.2 μm and 5 μm particles, the agreement is good and the particle stream width indeed approximately scales with the square of particle diameter. For particles larger than 8 μm the model predicts a full-width deflection and so the particle stream width becomes equal to the particle diameter. This prediction is also verified by the

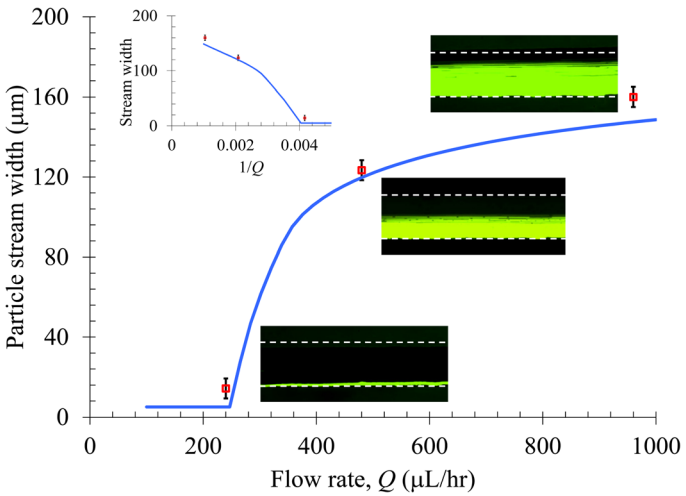

FIG. 6. Flow rate effect on the horizontal deflection of 5 μm diamagnetic particles in 0.5 × EMG 408 ferrofluid. The symbols represent the experimental data of particle stream width measured from the corresponding top-view superimposed images. The curve is obtained from the 3D analytical model. The inset graph shows the particle stream width vs. the inverse of the flow rate.

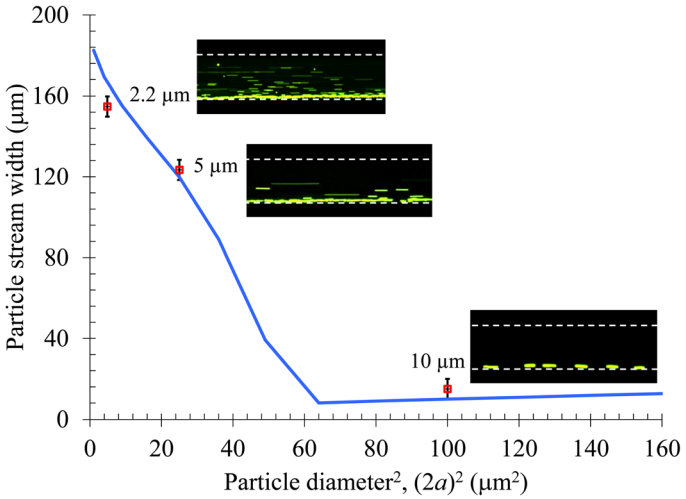

FIG. 7. Particle size effect on the magnetic deflection in 0.5 × EMG 408 ferrofluid at a flow rate of 480 μL/hr. The symbols represent the experimental data of particle stream width measured from the corresponding top-view superimposed images (only snapshot images are exhibited). The curve is obtained from the 3D analytical model.

experimentally measured stream width of 10 μm particles, where in the inset top-view image all particles line the channel sidewall.

4. Effect of ferrofluid concentration

The volume concentration of magnetic nanoparticles, ϕ, affects the magnetization, $\mathbf{M}_f$, and viscosity, η, of ferrofluids, both of which are involved in Eq. (10) for magnetophoretic particle velocity. For simplicity, we neglect the magnetoviscous effects[64] and treat η as a linear function of ϕ via $\eta = 10^{-3} + \phi/60$ (kg/m/s) in order to match the reported experimental value, 1.2×10^{-3} kg/m/s, for the original EMG 408 ferrofluid ($\phi = 1.2\%$).[57] The viscosities for $0.5 \times$ (i.e., $\phi = 0.6\%$) and $0.25 \times$ (i.e., $\phi = 0.3\%$) EMG 408 ferrofluids are therefore calculated as 1.1 and 1.05 ($\times 10^{-3}$ kg/m/s), respectively. As $\mathbf{M}_f$ scales linearly with ϕ [see Eq. (2)] which is to a greater extent than the according change in η, the diamagnetic particle deflection in ferrofluids is expected to be approximately proportional to ϕ. This analysis is verified by Fig. 8, where the

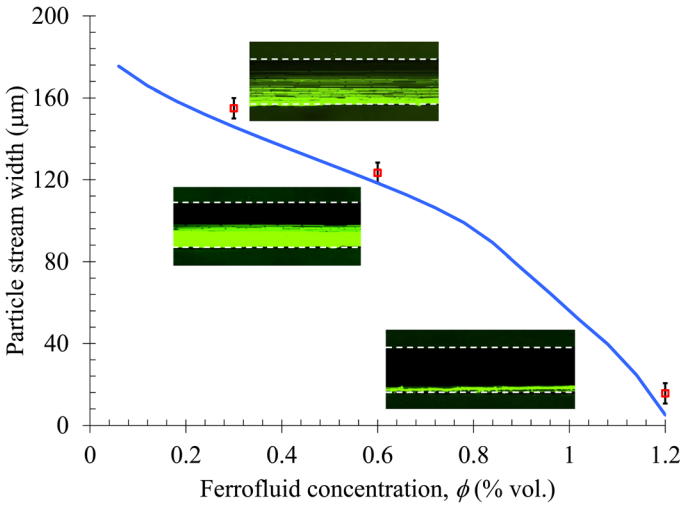

FIG. 8. Ferrofluid concentration (i.e., the volume fraction of magnetic nanoparticles) effect on the diamagnetic deflection of 5 μm particles at a flow rate of 480 μL/hr. The symbols represent the experimental data of particle stream width measured from the corresponding top-view superimposed images. The curve is obtained from the 3D analytical model.

experimentally measured stream widths of 5 μm particles in ferrofluids of the above three concentrations (symbols and the inset images) closely match the theoretical prediction (curve).

V. CONCLUSION

We have performed a systematic study of diamagnetic particle deflection in ferrofluid flows through a rectangular microchannel. It is found that diamagnetic particles can be deflected both outwards and downwards over the channel cross-section, forming a focused particle stream flowing near the corner that is the farthest to the center of the magnet and thus bears the smallest magnetic field. This three-dimensional deflection grows as particles approach and move by the magnet, where the effective range is within about 2 mm distance before and after the magnet in our experiment. The eventual particle deflection in the channel width direction has been observed to increase with the decrease of flow rate or the increase of ferrofluid concentration and particle size. We have also developed a three-dimensional analytical model to understand and simulate the diamagnetic particle deflection in ferrofluid flows. The theoretical predictions are found to agree with the experimental results quantitatively. It is anticipated that the demonstrated particle deflection in the horizontal and vertical planes of the microchannel may be exploited to realize a three-dimensional focusing of cells for microflow cytometry applications.

ACKNOWLEDGMENTS

This work was partially supported by Clemson University through a start-up package.

[1]X. Xuan, J. Zhu, and C. Church, Microfluid. Nanofluid. **9**, 1 (2010).
[2]J. Nilsson, M. Evander, B. Hammarstrom, and T. Laurell, Anal. Chim. Acta **649**, 141 (2009).
[3]N. Pamme, Lab Chip **7**, 1644 (2007).
[4]A. Lenshof and T. Laurell, Chem. Soc. Rev. **39**, 1203 (2010).
[5]P. K. Wong, T. Wang, J. H. Deval, and C. M. Ho, IEEE/ASME Trans. Mechatron. **9**, 366 (2004).
[6]O. D. Velev and K. H. Bhatt, Soft Matter **2**, 738 (2006).
[7]R. Pethig, Biomicrofluidics **4**, 022811 (2010).
[8]T. Laurell, F. Petersson, and A. Nilsson, Chem. Soc. Rev. **36**, 492 (2007).
[9]Z. Wang and J. Zhe, Lab Chip **7**, 1280 (2011).
[10]J. Friend and L. Y. Yeo, Rev. Mod. Phys. **83**, 647 (2011).
[11]N. Pamme, Lab Chip **6**, 24 (2006).
[12]G. Friedman and B. Yellen, Curr. Opin. Colloid Interface Sci. **10**, 158 (2005).
[13]R. M. Erb and B. Yellen, *Nanoscale Magnetic Materials and Applications*, edited by J. P. Liu (Springer, New York, 2009), p. 563.
[14]S. H. Cho, J. M. Godin, C. Chen, W. Qiao, H. Lee, and Y. Lo, Biomicrofluidics **4**, 043001 (2010).
[15]D. Erickson, X. Serey, Y. F. Chen, and S. Mandal, Lab Chip **11**, 995 (2011).
[16]H. Hwang and J. K. Park, Lab Chip **11**, 33 (2011).
[17]N. Pamme and A. Manz, Anal. Chem. **76**, 7250 (2004).
[18]M. A. M. Gijs, Microfluid. Nanofluid. **1**, 22 (2004).
[19]N. Pamme and C. Wilhelm, Lab Chip **6**, 974 (2006).
[20]J. D. Adams, P. Thévoz, H. Shea, H. Bruus, and H. T. Soh, Appl. Phys. Lett. **95**, 254103 (2009).
[21]B. D. Plouffe, L. H. Lewis, and S. K. Murthy, Biomicrofluidics **5**, 013413 (2011).
[22]F. Paul, S. Roath, D. Melville, D. C. Warhurst, and J. O. S. Osisanya, Lancet **2**, 70 (1981).
[23]K. H. Han and A. B. Frazier, Lab Chip **6**, 265 (2006).
[24]C. Liu, T. Stakenborg, S. Peeters, and L. Lagae, J. Appl. Phys. **105**, 102011 (2009).
[25]M. A. M. Gijs, F. Lacharme, and U. Lehmann, Chem. Rev. **110**, 1518 (2010).
[26]R. E. Rosensweig, AIAA J. **4**, 1751 (1966).
[27]K. A. Mirica, S. S. Shevkoplyas, S. T. Phillips, M. Gupta, and G. M. Whitesides, J. Am. Chem. Soc. **131**, 10049 (2009).
[28]A. I. Rodríguez-Villarreal, M. D. Tarn, L. A. Madden, J. B. Lutz, J. Greenman, J. Samitier, and N. Pamme, Lab Chip **11**, 1240 (2011).
[29]M. D. Tarn, N. Hirota, A. Hes, and N. Pamme, Sci. Technol. Adv. Mater. **10**, 014611 (2009).
[30]A. Winkleman, K. L. Gudiksen, D. Ryan, and G. M. Whitesides, Appl. Phys. Lett. **85**, 2411 (2004).
[31]S. A. Peyman, E. Y. Kwan, O. Margarson, A. Iles, and N. Pamme, J. Chromatogr. A **1216**, 9055 (2009).
[32]J. H. Kang, S. Choi, W. Lee, and J. K. Park, J. Am. Chem. Soc. **130**, 396 (2008).
[33]Y. K. Hahn and J. K. Park, Lab Chip **11**, 2045 (2011).
[34]H. Watarai and M. Namba, Anal. Sci. **17**, 1233 (2001).
[35]H. Watarai and M. Namba, J. Chromatogr. A **961**, 3 (2002).
[36]H. Watarai, M. Suwa, and Y. Iiguni, Anal. Bioanal. Chem. **378**, 1693 (2004).
[37]A. Winkleman, R. Perez-Castillejos, K. L. Gudiksen, S. t. Phillips, M. Prentiss, and G. M. Whitesides, Anal. Chem. **79**, 6542 (2007).
[38]K. A. Mirica, S. T. Phillips, S. S. Shevkoplyas, and G. M. Whitesides, J. Am. Chem. Soc. **130**, 17678 (2008).
[39]K. A. Mirica, S. T. Phillips, C. R. Mace, and G. M. Whitesides, J. Agric. Food Chem. **58**, 6565 (2010).

[40]M. Suwa and H. Watarai, Anal. Chim. Acta **690**, 137 (2011).
[41]R. E. Rosensweig, Annu. Rev. Fluid Mech. **19**, 437 (1987)
[42]M. D. Krebs, R. M. Erb, B. B. Yellen, B. Samanta, A. Bajaj, V. M. Rotello, and E. Alsberg, Nano Lett. **9**, 1812 (2009).
[43]A. Kose, B. Fischer, L. Mao, and H. Koser, Proc. Natl Acad. Sci. **106**, 21478 (2009).
[44]S. A. Sharpe, "Magnetophoretic cell clarification," Ph.D. dissertation (MIT,2004).
[45]S. K. Fateen, "Magnetophoretic focusing of submicron particles dispersed in a polymer-stabilized magnetic fluid," Ph.D. dissertation (MIT, 2002).
[46]B. B. Yellen, G. Friedman, and A. Feinerman, J. Appl. Phys. **93**, 7331 (2003).
[47]B. B. Yellen and G. Friedman, Langmuir **20**, 2553 (2004).
[48]B. B. Yellen, O. Hovorka, and G. Friedman, Proc. Natl Acad. Sci. **102**, 8860 (2005).
[49]B. B. Yellen, R. M. Erb, D. S. Halverson, O. Hovorka, and G. Friedman, IEEE Trans. Magn. **42**, 3548 (2006).
[50]D. Halverson, S. Kalghatgi, B. Yellen, and G. Friedman, J. Appl. Phys. **99**, 08P504 (2006).
[51]R. M. Erb and B. B. Yellen, J. Appl. Phys. **103**, 07A312 (2008).
[52]R. M. Erb, H. S. Son, B. Samanta, V. M. Rotello, and B. B. Yellen, Nature **457**, 999 (2009).
[53]K. H. Li and B. B. Yellen, Appl. Phys. Lett. **97**, 083105 (2010).
[54]V. N. R. Annavarapu, "Size based separation of submicron nonmagnetic particles through magnetophoresis in structured obstacle arrays," Ph.D. dissertation (MIT, 2010).
[55]E. Feinstein and M. Prentiss, J. Appl. Phys. **99**, 064901 (2006).
[56]T. Zhu, F. Marrero, and L. Mao, Microfluid. Nanofluid. **9**, 1003 (2010).
[57]T. Zhu, D. J. Lichlyter, M. A. Haidekker, and L. Mao, Microfluid. Nanofluid. **10**, 1233 (2011).
[58]L. Liang, Y. Ai, J. Zhu, S. Qian, and X. Xuan, J. Colloid Interface Sci. **347**, 142 (2010).
[59]R. E. Rosensweig, *Ferrohydrodynamics* (Cambridge University Press, Cambridge, 1985).
[60]E. P. Furlani, *Permanent Magnet and Electromechanical Devices: Materials, Analysis, and Applications* (Academic, New York, 2001).
[61]F. M. White, *Viscous Fluid Flow* (McGraw-Hill Science/Engineering/Math, New York, 1991).
[62]J. Happel and H. Brenner, *Low Reynolds Number Hydrodynamics* (Prentice-Hall, Englewood Cliffs, NJ, 1973).
[63]D. Di Carlo, D. Irimia, R. G. Tompkins, and M. Toner, Proc. Natl. Acad. Sci. **104**, 18892 (2007).
[64]S. Odenbach, *Magnetoviscous Effects in Ferrofluids* (Springer, New York, 2002).